A Morphing Cargo Drone for Safe Flight in Proximity of Humans

Przemyslaw Mariusz Kornatowski, Mir Feroskhan, William J. Stewart, and Dario Floreano, *Senior Member, IEEE*

***Abstract*—Delivery drones used by logistics companies today are equipped with unshielded propellers, which represent a major hurdle for in-hand parcel delivery. The exposed propeller blades are hazardous to unsuspecting bystanders, pets, and untrained users. One solution to provide safety is to enclose a drone with an all-encompassing protective cage. However, the structures of existing cage designs have low density in order to minimize obstruction of propeller airflow, so as to not decrease efficiency. The relatively large openings in the cage do not protect hands and fingers from fast rotating propellers. Here we describe a novel approach to safety and aerodynamic efficiency by means of a high-density cage and morphing arms loosely inspired by the box turtle. The drone cage is made of a dense and lightweight grid. When flying in proximity of humans, the arms and propellers are retracted and fully sealed within the cage, thus making the drone safe and also reducing the total footprint. When flying at cruising altitude far from people and objects, the arms and propellers extend out of the protective grid, thus increasing aerodynamic efficiency by more than 20%.**

***Index Terms*—Aerial systems, applications, intelligent transportation systems, field robots, logistics.**

I. Introduction

DRONES are becoming an increasingly useful tool to deliver parcels faster [1], greener [2], and cheaper [3] to previously inaccessible places. As a result, several logistics companies [4]–[7] are considering using drones for e-commerce markets. However, most of these deliveries tend to employ bulky drone platforms designed for stable, long-range dispatch and require designated take-off and landing spaces. Additionally, user access to these spaces are restricted during operation to avoid harm posed to bystanders due to exposed propellers. Moreover, delivery to places where there is no space to land, e.g. a window or balcony, delivery to people stuck in a traffic jam or inclined environments is impossible for drones. Together, these challenges remove the possibility of person-to-person and last-centimeter deliveries where packages can be safely delivered directly to the recipient's hands or hard-to-reach, cluttered locations.

In the context of ensuring safe handling for last-centimeter delivery, one approach is to encase the propellers in a protective cage [8]–[13]. A highly dense cage structure enhances safety [14] by preventing users from accessing the propellers. However, high density cages incur a high drag penalty [15] and decreased available lift [10]. The alternative, a low-density cage structure would allow small external objects, such as fingers or hands, access to propellers, which could be dangerous for people and animals. Additionally, to reduce the added weight of the cage, the vehicle volume is kept low by shortening the arm length of the quadcopter.

However, this reduces the drone's stability due to the lower mass moment of inertia [16], and also decreases its efficiency since a larger change in thrust is required to tilt the drone. Therefore, a higher change in rotation speed of propellers is needed and more power is consumed.

In this letter, we present a novel approach to safety and efficiency for delivery drone design. We propose to enclose a quadcopter (Fig. 1(A)–(B)) in a safe, densely gridded cage based on a tennis-racket stringing technique [17]. To overcome the drag penalty of such a cage, the quadcopter has a morphing capability inspired by box turtles' (Terrapene carolina, T. ornata) limb retraction for protection (Fig. 1(C)–(D)) [18]–[20]. The quadcopter can retract its arms into the cage during take-off and landing to prevent access to its propellers, keeping people safe. In addition to preventing injury, the retractable arms strategy results in a smaller footprint of the quadcopter during take-off and landing, offering access to cluttered and hard-to-reach places. In the proposed solution, the parcel is strategically located on top of the drone.

This approach, as suggested in [21], enables the propellers to be tightly packed together into the cage without the parcel blocking the slipstreams. This allows the volume of the cage structure to be minimized by overlapping the propellers as shown in Fig. 2(C). The overall small vehicle volume provides better portability and storage with the arms fully retracted (Fig. 2). The cage structure also replaces the need for landing gear. During cruise flight, the arms of the quadcopter can be extended out of its cage, giving it the associated increase in efficiency and stability. Based on this proposed design, the mission profile of a drone, illustrated in Fig. 1(E), consists of the propellers contained inside the cage only during take-off and landing (just a small portion of the whole mission) and deployed outside the cage during cruise to increase aerodynamic efficiency.

Manuscript received February 22, 2020; accepted April 21, 2020. Date of publication May 11, 2020; date of current version May 25, 2020. This letter was recommended for publication by Associate Editor P. Pounds and Editor J. Roberts upon evaluation of the reviewers' comments. This work was supported by the Swiss National Science Foundation through the National Centre of Competence in Research (NCCR) Robotics and armasuisse. *(Corresponding author: Przemyslaw Mariusz Kornatowski.)*

Przemyslaw Mariusz Kornatowski, William J. Stewart, and Dario Floreano are with the Laboratory of Intelligent Systems, School of Engineering, Ecole Polytechnique Federale de Lausanne, Lausanne CH1015, Switzerland (e-mail: przemyslaw.kornatowski@epfl.ch; william.stewart@epfl.ch; dario.floreano@epfl.ch).

Mir Feroskhan is with the School of Mechanical and Aerospace Engineering, Nanyang Technological University, Singapore 639798, Singapore (e-mail: mir.feroskhan@ntu.edu.sg).

This letter has supplementary downloadable material available at https://ieeexplore.ieee.org, provided by the authors.

Digital Object Identifier 10.1109/LRA.2020.2993757

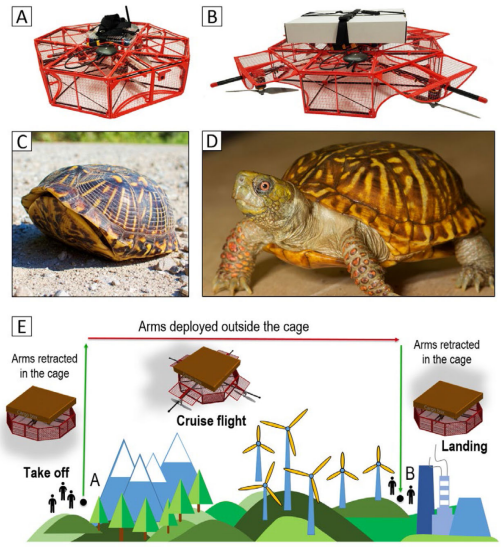

Fig. 1. GearQuad, the morphing quadcopter that is fully enclosed in a cage enhancing safety for children and animals. (A) Photo of the retracted arms configuration inside the cage for take-off and landing. (B) Photo of the arms deployed outside the cage for the cruise mode with a parcel. (C) A 'box turtle' with retracted limbs and closed shell for protection [18]. (D) A box turtle with deployed limbs for locomotion [19]. (E) The concept of safe and efficient delivery by a quadcopter with retractable arms. (Green arrow) The arms retracted in the cage during take-off and landing mode – while close to people and animals. (Red arrow) The arms deployed out of the cage for efficient cruise mode – far away from people and obstacles.

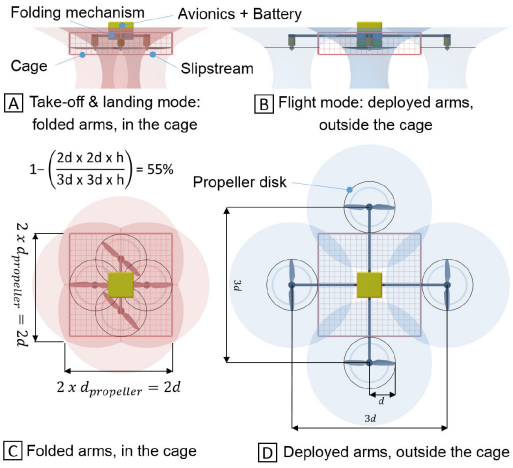

Fig. 2. (A–B) Side cross-section of the quadcopter with the parcel and the cage. (C–D) Top view of the quadcopter without the parcel. (A, C) Retracted safe mode: arms inside the cage for take-off and landing. (B, D) Deployed mode for the cruise flight: arms deployed outside the cage. Increased efficiency, not affected by the grid of the cage.

II. Cage Design

The design of a safety cage that simultaneously protects humans and does not obstruct the propeller airflow, requires addressing multiple conflicting design challenges. The first challenge is that the cage should be dense enough to prevent even small children's fingers from passing through and touching the fast-moving propellers. The second is that the cage should be stiff enough to prevent deformation resulting in contact with the propellers when people grab it. Lastly, the cage should minimally disturb the airflow through the propellers.

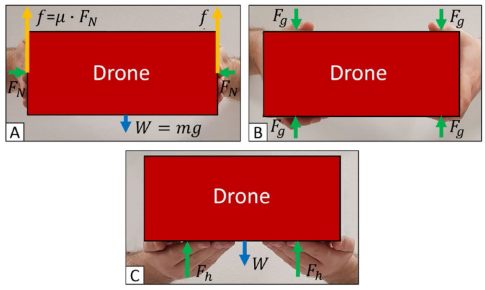

Fig. 3. Free body diagrams of the drone cage held by the user in three different lading situations (side view). (A) Drone held between user's open palms. (B) Drone gripped by user's palms. F_h is holding force, W is the drone weight, m is the drone mass, g is gravitational acceleration, f is friction force, F_N is the normal contact force, μ is the friction coefficient between the cage material (plastic) and human skin (0.7 [25]), F_g is the gripping force. (C) Drone held on top of a user's palms.

To minimally affect the airflow from the propellers and reduce drag during take-off and landing, thickness of the grid strings should be minimized. Multicopters typically fly in a variety of orientations and inclinations within a single mission. Thus, the strings should have a symmetrical cross-section to keep the same drag coefficient regardless of attitude. To fulfill this requirement, a circular cross-section was selected. To reduce the drag, the thickness of cylinders should be minimized, but thinner cylinders are more flexible and may allow the cage to deform contact the spinning propellers. Therefore, this tradeoff requires a study of the appropriate thickness and choice of materials. To do that, the forces applied on the cage while the drone is flying close to people and during in-hand landing need to be defined.

To fulfill the above-mentioned requirements, we designed a stringed cage inspired by a tennis racket that consists of a rigid frame and stretched strings that provide rigidity with very small deformation to the stiffness of the tensioned strings.

A. Grid Density

The density of the cage was designed such that the gaps in the cage were small enough that a child could not put his fingers into the cage. As a reference, statistical data of three-year-old children's smallest finger was selected [22]–[24] and the diameter of the fingertips (distal phalanges) was used. The diameters ranged from 9 to 10 mm. Moreover, to enhance safety, one millimeter was subtracted from this diameter. The resulting maximal open space in the grid is 8 mm. This density ensures that the drone is safe when used near children.

B. The Cage and Grid Stiffness

The hallmark of multicopter safety is being safe enough for the user to catch the vehicle in flight. For this letter, we therefore use the scenario of in-hand landing as a goal for user safety. A pair of outstretched hands can withstand a load of up to 20 kg without risk of injury [23]. For in-hand landing, a safety factor of 5 is applied on the gross weight limit of the delivery vehicle. We focused on three possible in-hand landing situations (Fig. 3).

In situation A, the drone is caught from the sides, between the user's open palms flushed against the drone (Fig. 3(A)). Here, the friction forces f generated between the palms and the cage bear the drone weight W. Therefore, the required contact normal force F_N applied by the user's palms is $W/(2\mu)$ and is

independent of the surface area of the palms. For example, a 2.5 kg drone with a friction coefficient μ of 0.7 (between human skin and a polyester material) [25], the required normal force F_N is 17.5 N. Therefore, as the cage is held by two hands, the maximum force that the 2.5 kg cage needs to withstand without being deformed is 35 N.

In situation B, the user grasps the drone with both palms, mainly the fingers (Fig. 3(B)). To determine the gripping forces acting on the cage as the user grasps the drone, we assume that the weight of the drone is borne by the user's arm muscles. A study from [23] indicated the maximum average gripping force applied by one's palms when gripping an object between 3.5 and 9.5 cm thick. For instance, for a cage with 7.5 cm thickness, the average gripping force applied is about 300 N. The magnitude of the gripping force also depicts a downward trend as the thickness increases. Therefore, a drone that is thicker would experience a smaller gripping force during in-hand landing.

Thus, 300 N ($2 \cdot F_g$) would be a conservative approximation of the force that a user would apply when grasping a landing caged multicopter with more than 7.5 cm thickness.

In situation C, the drone lands on top of the user's outstretched palms, perpendicular to his body (Fig. 3(C)). Here, the drone structure should be able to bear its own W weight force. Since situation C is comparable to situation B when the force is applied to the cage frame and is the least demanding in terms of the force applied, only situations A and B are tested in the experimental validation for in-hand landing in Section IV.

C. Drag Calculations of a Grid

The drag generated by the grid in the propeller slipstream and in the incident airflow during cruise flight can be calculated using the drag coefficient for obstructions in a wake, called the wake loss factor [26]. The wake loss factor for cylindrical shaped obstructions can be written as:

$$C_{dw} = \beta \cdot C_d \tag{1}$$

where β is the blockage factor:

$$\beta = \frac{\text{projected area of obstructing cylinders}}{\text{total area of the wake}} \tag{2}$$

C_d is the drag coefficient of the cylinders [27], [28], which is a function of their local Reynolds numbers. The projected area of obstructing cylinders can be calculated knowing the space between strings and the diameter of the strings.

The Reynolds number can be calculated from:

$$Re = \frac{\rho \cdot u \cdot L}{\mu} \tag{3}$$

where, ρ is the density of the air (1.225 kg/m^3), u is the velocity of the air with respect to the object obstructing the flow [m/s], L is a characteristic linear dimension [m], and μ is the dynamic viscosity of the air (18.5 μPa·s). For small diameters of cylinders (0.1–1 mm) and low airspeeds ($\sim$ 25 m/s), the local drag coefficient will typically range between 0.95 and 1.65 [28].

Because of the uniform grid density, the blockage factor is simply the grid density. This means that it is independent of wake area. Combining this with the drag coefficient, C_d gives the wake loss factor. In the case where the wake loss factor is too high, the string diameter should be reduced and stronger material found to provide enough strength. The lift reduction equations presented here will be validated experimentally in Section IV.

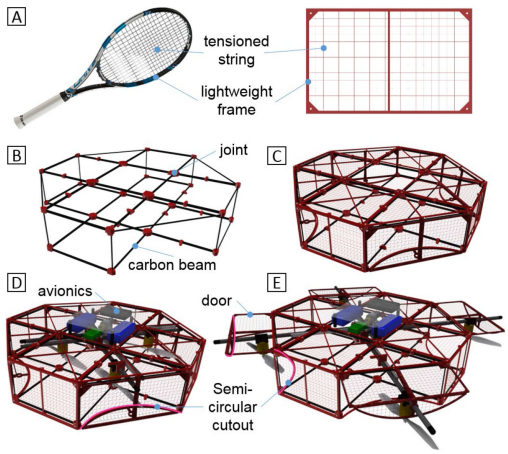

Fig. 4. Elements of the GearQuad. (A) Comparison between a tennis racket and a drone grid module. (B) Truss structure of the cage composed of pultruded carbon fibre beams connected by plastic joints. (C) Truss structure with grid modules installed. (D) The cage with integrated rotor arms and avionics payload. The arms are retracted inside the cage. (E) The drone with deployed arms and opened doors.

III. Implementation

To validate the proposed concept, we designed and characterized a 2 kg, morphing, densely-caged quadcopter, codenamed GearQuad, capable of carrying 500 g payload.

A. Cage

The cage is composed of two elements: external grid modules of different sizes and shapes (Fig. 4(A)) and an internal carbon truss (Fig. 4(B)). The grid modules are attached to the outside of the carbon truss (Fig. 4(C)). The truss is composed of 6 $\times$ 1 mm carbon fiber beams glued together with 3D printed joints. Thus, the carbon truss provides rigidity to the cage.

The grid module was designed following the procedure presented in Section II and validated experimentally in Section IV. The grid modules (Fig. 4(A)) consist of tensioned string (0.3 mm diameter Dyneema string, 336.5 N at the break (tensile strength)) threaded through 3D printed, stiff, and lightweight plastic frames (PLA). The string was threaded into an 8 mm by 8 mm grid through 1 mm diameter holes drilled in the frame. The strings were glued to each other using cyanoacrylate glue to prevent them from sliding if a finger is placed between them. The added glue increased the string diameter to 0.35 mm. The plastic module was attached with M2 screws to the plastic joints of the truss. The bottom part of the cage has semi-circular cutouts as presented in Fig. 4(E). The semi-circular cutouts ensure that the grid does not impede the propeller slipstreams when the propellers extend fully. In addition, these cutouts reduce the time required to deploy and retract the arms by decreasing the distance the propellers must travel to reach clean air. Therefore, a shorter arm length is implemented which reduces weight and drag.

The vehicle has the dimensions 52 $\times$ 52 $\times$ 14.5 cm with the arms retracted and 86 $\times$ 86 $\times$ 14.5 cm with the arms deployed. The dimensions of the drone are the result of two design decisions: (i) the propellers should provide sufficient thrust to lift the drone with a 500 gram payload; (ii) the maximum size of the drone with its arms retracted should fit within a person's arm's length (with his hands outstretched, perpendicular to his body). For a small British adult (44 kg body weight), the length between

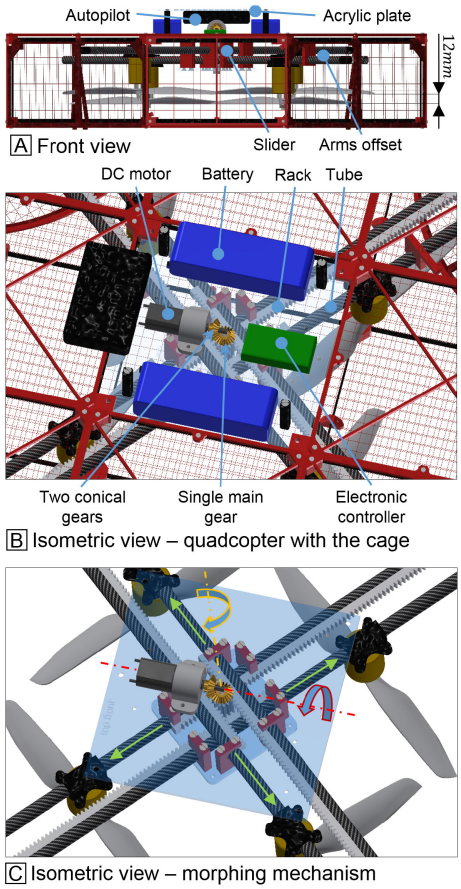

Fig. 5. Details of the propulsion mechanisms and morphing mechanism of the drone. (A) Side view of the drone presenting the offset of the arms placed in the plastic sliders. (B) Magnified isometric view of the drone showing the morphing arms mechanism and avionics. (C) The morphing mechanism of the arms shown without the cage and avionics. The blue arrows show the direction of rotation of the conical gears about the motor axis (red dashed line) and gear axis (yellow dashed line). The green arrows show the direction of arms deployment. Reversing the direction of rotation of the motor will change the direction of translational movement of the arms.

the outstretched palm and chest is 34.5 cm [23], which is more than half of the length of the drone. This allows the drone to be grabbed by the recipient when landing.

The cage was intentionally designed with the shape of an octagon instead of a square to reduce the total mass of the material. Four doors are located at the four perpendicular sides of the cage. The doors are pushed open by the arms of the quadcopter on deployment (Fig. 4(E)) and are automatically closed by springs when the arms are retracted into the cage.

B. Morphing Drone

To minimize the size of the cage, and thus its weight and drag, the propeller disks were vertically offset by 12 mm, as shown in Fig. 5(A), which allows overlapping between the propellers (Fig. 2(C)). This is a key design feature to reduce the quadcopter cage footprint to a minimum. One of the challenges of designing the morphing technique is to limit the number of actuators deploying the arms of the quadcopter without compromising the mechanical strength of the arms. As a result, we designed a new, innovative mechanism that deploys the four arms symmetrically and simultaneously (Fig. 5(B)–(C)).

TABLE I
MASS DISTRIBUTION OF THE MORPHING MECHANISM

Component	Mass [g]
4 x racks	39
gears + shaft + bearings	21
longer arms to open the doors	53
2 x switch	4
motor	45
controller	8
TOTAL MASS OF MORPHING MECHANISM	**169**

TABLE II
MASS DISTRIBUTION OF THE PROTOTYPE

Component	Mass [g]
folding mechanism	169
quadcopter	1193
battery	344
cage	377
payload	500
TOTAL MASS OF QUADCOPTER	**2583**

The main body of the mechanism (Fig. 5(B)) is made out of 5 mm thick laser cut acrylic plates. The arms consist of 10 mm carbon fiber tubes with a wall thickness of 1 mm. Each arm was inserted into a plastic, 3D printed (ABS) lubricated sliders that allows the arms to deploy and retract freely (Fig. 5(C)). To move the arms, a plastic rack was glued to each arm using cyanoacrylate glue. The rack is engaged by a single main gear placed in the center of the drone between the arms (Fig. 5(B)–(C)). Thus, when the gear rotates, all four arms simultaneously deploy or retract (Fig. 5(C)). To rotate the main gear, a DC motor (Pololu 154:1 Metal Gearmotor 20D $\times$ 44L mm) was used. To ensure a compact design, the motor is mounted perpendicular to the main gear of the mechanism deploying the arms. Two conical gears (Fig. 5(B)–(C)) connect the motor and the single main gear.

An electronic controller (Pololu Simple High-Power Motor Controller 24v12) to control the speed and direction of rotation of the motor is connected to the autopilot's PWM output. Moreover, two end switches are connected to the controller. The switches are responsible for turning off the DC motor when the limit positions are reached.

As shown in Tables I and II, the elements that allow extension of the arms amount to 6.5% of the gross weight of the drone.

IV. EXPERIMENTAL CHARACTERIZATION

A series of experiments was performed to validate the influence of the grid and of the entire cage (including reinforcing elements) on lifting capabilities of the drone as predicted by the calculations described in Section II(C).

In the experiments, lift was measured at varying distances (d) between a grid and a single propeller in two configurations (Fig. 6). In the first configuration, the grid is downstream of the propeller (Fig. 6(A)). To test this configuration, the grid was installed below the propeller as shown in Fig. 6(A) and the setup shown in Fig. 6(D) was implemented. In the second configuration, the grid is upstream of the propeller (Fig. 6(B)). This represents the case where the grid modules are positioned above the propellers on the quadcopter. To test both configurations, the characterization bench shown in Fig. 6(D) was used, however, the propeller orientation was changed (flipped 180

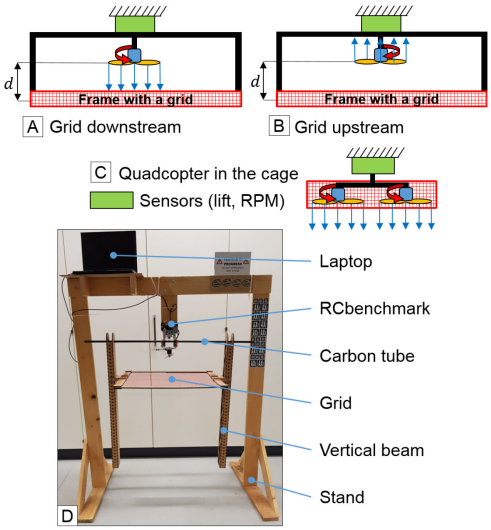

Fig. 6. Experimental setup for lift measurements. The blue arrows represent the direction of the airflow. The red arrows represent the direction of the rotation of propellers. (A) A schematic representation of the setup with the grid placed downstream of a single propeller. (B) A schematic representation of the setup with the grid placed upstream of a single propeller. (C) A schematic representation of the setup with the arms retracted quadcopter with a cage. (D) Photo of the experimental set-up with a grid attached to 60x60 cm square wooden frame.

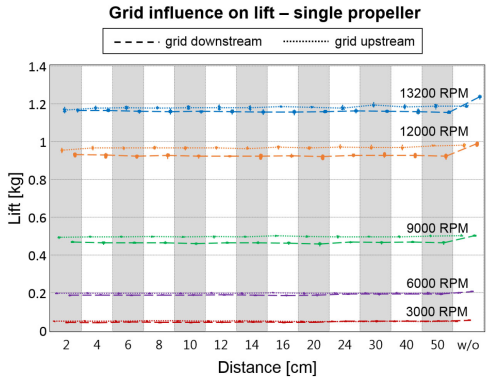

Fig. 7. Influence on lift when a grid is placed downstream (dashed line) and upstream (dotted line) of a single propeller - APC8x4.5MR. Measurements are made for different rotation speeds of the motor. The grid is placed at different distances from the propeller.

degrees around the horizontal axis) and direction of rotation was reversed. This allows the grid in the setup to remain in the position below the propeller, as shown in Fig. 6(B). In addition, for distance between the propeller and grid, studies on the dependency of rotation speed and propeller size were also performed by repeating the experiment at various rotation speeds and propeller sizes.

The measurements were conducted using the RC Benchmark 1580 Series dynamometer sensor, which gives values in kg [29], attached to a custom stand (Fig. 6(D)). During the experiment, an AXI 2217-16 V2 (1380KV) motor with 40A ESC was used. The voltage was set to 12.6V with a power supply (Keithley 2260B-30-72) corresponding to the equivalent of a fully charged 3S battery. The grid is stretched into a square frame with external dimensions of 60 cm and internal dimensions of 54 cm. The grid is composed of 0.3 mm strings with 8 mm spacing in between. The frame is connected to the RC benchmark sensor by a 10 mm carbon tube and two vertical beams (Fig. 6(D)). The sensor is attached to the center of the stand using screws. The grid is moved from a distance of 2 cm to 50 cm from the propeller, with measurements taken at thirteen different steps in between. The values of distances are presented on the x-axis of the plot in Fig. 7. The experiment was conducted for the two specified configurations (grid positioned upstream and downstream of propeller) and for the case without the grid.

As shown in Fig. 7, the grid placed at the aforementioned distances upstream of an 8 $\times$ 4.5MR propeller reduces the lift by an average value of 6.5 g or 0.6% of the measured for a single propeller rotating at 13200 RPM upstream of the grid. On the other hand, the grid placed downstream of the single propeller rotating at 13200 RPM, decreases the lift by an average value of 78 g or 6.3%. The value of decrement for both configurations is constant for varying distances between the grid and propeller. Therefore, varying the distance between the grid and the propeller does not have a measurable influence on the electric power consumed by the motor.

For the downstream configuration, the wake loss factor can be calculated using equation (1) and then compared with the experimental results. Based on the string diameter and spacing, the blockage factor β calculated using (2) is 0.070. The Reynolds number, calculated from (3), is approximately 477, which corresponds to a local drag coefficient of 1.1 [27], [28]. The air speed (24 m/s) used in the calculation of the Reynolds number was measured using a hot wire anemometer sensor.

The sensor was placed 2 cm below the propeller without the grid and at a distance equal to half of the propeller radius from the axis of rotation of the motor. Using these values, the wake loss factor calculated with equation (1) gives a value of 0.0776.

This value of the wake loss factor can be compared to an experimentally determined value by comparing the motor thrust with and without the grid using the formula:

$$C_{\text{dw experimental}} = 1 - \frac{\text{thrust}_{\text{with grid}}}{\text{thrust}_{\text{without grid}}}. \tag{4}$$

This experimentally determined value is approximately 0.0777. Thus, calculations (0.0776) match well with experimental validation (0.0777).

This wake loss factor calculation was also validated using a higher density grid composed of 1.5 mm strings separated by 1.5 mm spacing in between. The calculated blockage factor β of 0.7087 concurs with the experimental value of 0.6950 (the Reynolds number calculated is approximately 2384, which corresponds to a local drag coefficient of 0.95).

For the setup where the grid is upstream of the propeller (Fig. 6(B)), the airflow is pressing on the load cell, which creates an additional force on the load cell. This force must be accounted for to compare measurements to those obtained when the grid is downstream of the propeller. Thus, the drag value generated by the setup was measured and added to the values of lift measured in the upstream grid configuration. Wake loss factor was not calculated for the upstream configuration as the grid is not in the wake of the propeller for this configuration.

A. *Lift Savings With Deployed Arms of Quadcopter*

The grid placed below and above a propeller has minimal impact on lift (<10%). However, the cage placed around the quadcopter and the truss carbon structure with overlapping propellers generate additional drag and turbulence that reduce lift.

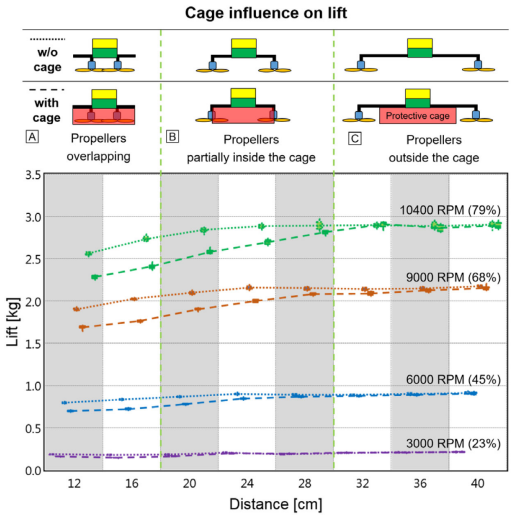

Fig. 8. Influence on lift for a quadcopter with and without the cage in different arms deployment configurations. At the top of the figure are quadcopters in different phases of arms deployment, indicating graphically the state of the quadcopter corresponding to the plot below. Images above the plot show three phases of deployment. (A) propellers overlapping and fully in the cage, (B) propellers partially in the cage, (C) propellers outside the cage. Distance of deployment was measured from yaw axis of the drone to the rotation axis of a propeller. On the graph, the dotted lines present plots for the drone without the cage (nominal case), while the dashed lines refer to the plots with the cage, at different RPM and percentage of full throttle (max. RPM).

Two experiments were performed to understand the impact of the entire cage (Fig. 6(C)), one with the quadcopter equipped with the cage and the second with the same quadcopter without the cage, established as the nominal case (Fig. 8). Both quadcopters were attached to the RC benchmark test stand used in the previous experiments. The lift was measured in different states of the arm deployment and with different motor speeds. The arm deployment distance was measured from the yaw axis of the drone to the axis of rotation of the propeller. In cruise flight, multicopters fly at a maximum of 80% of full throttle for maneuverability and energy efficiency. Measurements were therefore performed at 10400 RPM which is 79% of full throttle. As observed in Fig. 8, the lift of the drone without the cage (dotted lines) is only affected at its smallest configuration with completely retracted arms (distance 12–16 cm), where the neighboring propellers overlap and tips of the propellers are close to each other. As soon as the propellers move away from each other, the lift value increases and becomes constant. The difference in lift between fully retracted arms and fully deployed arms is 12% for the quadcopter without cage and 21% with the cage. This shows that as expected, the cage decreases the lift of the drone. In addition, these experiments showed that the lift has the same value when the propellers are outside the cage and with propellers placed at the same position but without the cage (plots converge). This result demonstrates that deploying the arms outside the cage provides unobstructed airflow and avoids negative impact on the lift that matches the nominal case.

B. Grid Strength for Finger Pressure

To validate the safety of the grid while a finger is pushed on the grid, an experiment with an artificial finger was performed. Of interest is how much force is required to deflect the grid 35 mm (the distance to the propeller tip) and how that compares

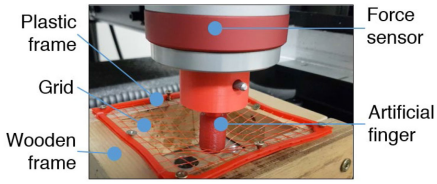

Fig. 9. Experimental setup installed in Instron machine for testing a grid module. During the tests an artificial 3D printed finger of the 19 mm diameter was used. The finger was applied between the strings of the grid.

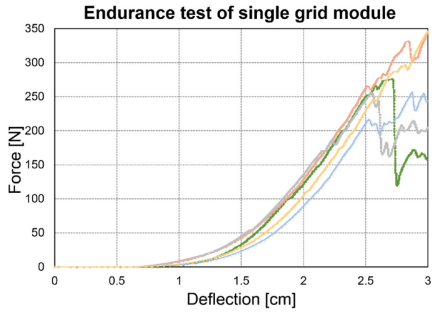

Fig. 10. Plot shows results of the experiment which tests the strength of the grid module when a finger presses between strings of the grid (each color represents a single test). The force is measured until the module breaks which occurs after 2.5 cm and reaching an average value of 297 N.

with the force applied by an adult of 22 to 30 years of age when catching the vehicle, which is 30 N [31].

To imitate a soft finger, a flexible cylinder with rounded edges, made of TPE (NinjaFlex) was 3D printed (Fig. 9). The size of the finger (19 mm in diameter) was selected from a population of British adults [30]. The artificial finger was mounted onto an Instron 5965 machine (with 500 N load cell), as shown in Fig. 10. The force required to break the single string used for the grid according to the manufacturer is 336.5 N, which is almost twelve times higher than the force applied by a male subject's index finger [30]. This means that the string used has a high safety factor and could be the last breaking point. Thus, other breaking points of the grid should be considered, which could be: (i) reaching a grid deflection of 35 mm; (ii) cracking of the plastic frame holding the grid; or (iii) separation of strings at grid vertices due to failure of the glue used to bind the strings. For characterizing those additional breaking points, an experiment was performed. The artificial finger was placed between the strings so that the force applied by the Instron machine would press the strings apart. For the test, 5 $\times$ 10 cm square modules, which correspond to the size of the modules used on the vehicle were 3D printed and threaded. The module was attached to a square wooden frame at the corners and at the middle of each side, the same way, as it is attached to the vehicle (Fig. 10).

Fig. 10 presents the results of the strength tests of five grid modules. Each color represents a single test. The average value of maximum load at breaking point is 297 N with standard deviation 46 N. Samples started to fail reaching average extension of 28 mm with standard deviation 2 mm. This number fulfils the previously presented required force of 30 N that can be applied by an index finger of adults between 22 and 30 years old [31]. Under a load of 30 N, the deflection is smaller than 1.5 cm, which is smaller than the 35 mm that separate the grid from the tip of the rotating propeller. During the test, the plastic frame broke three times and the glue broke two times.

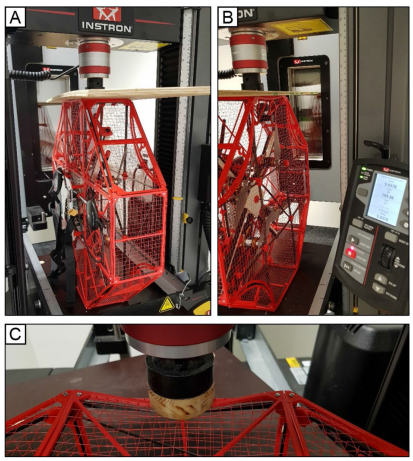

Fig. 11. The drone installed in the Instron machine to test deformation during in-hand landing. (A–B) The drone placed on its sides (vertical orientation) for the cage deformation test where the cage is held between two open palms. (A) Top view of the drone. (B) Bottom view of the drone. (C) The drone placed in the horizontal orientation for the cage deformation test where the cage is gripped by two palms – four fingers and thumb.

C. Cage Frame Strength While Landing in Hands

To enable in-hand delivery, the cage has to be rigid enough to prevent deformation and access to the propellers. To measure the maximum force applicable without bringing the cage in contact with the propellers, the two situations A and B from Section II were considered: (A) the drone is caught from the sides, between the user's open palms flushed against the drone (Fig. 3(A)); (B) drone is gripped at the sides by two palms, mainly the fingers (Fig. 3(B)).

For situation A, the drone platform was placed between two wooden plates and installed vertically in the Instron machine (Fig. 11(A)–(B)). The Instron applied a force from 0 N to 350 N. The experiment revealed that the structure of the cage can withstand on average 312 N (10 tests, standard deviation 8.1 N) before it experiences a deformation of at least 5 mm (distance between the propeller tips and the cage is 35 mm in the prototype), which is nine times greater than the 35 N force approximated for a 2.5 kg drone in Section II. The experiment was stopped after reaching 5 mm to prevent from damaging the prototype.

For situation B, where the drone is gripped between two palms while landing, the drone platform was placed horizontally in the Instron machine (Fig. 11(C)) between a plate and a force sensor, mimicking four fingers from the bottom and a thumb at the top. The cage deformation was measured at two locations. In the first location, the thumb was placed at the center of the sidewall of the drone (Fig. 11(C)). An applied force from the Instron machine of 300 N (a conservative approximation for a 14.5 cm cage thickness as indicated in Section II) deformed the cage by 9.5 mm (10 tests, standard deviation 0.6 mm). In the second location at the connection of two walls, the cage under the load of 300 N deformed by only 1.9 mm (10 tests, standard deviation 0.75 mm). Both tests revealed that the drone can be safely gripped because the minimum distance between the cage and a propeller in this direction is 2.5 cm.

D. Flight Stability During Morphing

In order to measure the stability of the drone during morphing, a series of deployment tests was performed in an OptiTrack motion capture system. The drone was commanded to hover in position at 0.7 m altitude. During hover, the arms were retracted and deployed. Default autopilot settings were taken from the PX4 flight stack controller for an X shaped quadcopter. Fig. 12 shows the position of the drone in x, y, z and roll, pitch, and yaw angles as a function of time. As the arms deploy and retract, the drone remains in position in the xy horizontal plane, but deviated by approximately 0.3 m along the vertical axis z (Fig. 12(A)). This altitude variation is generated by the influence of the cage on the lift force as the arms extend and retract. Fig. 12(B) shows the small oscillation around the pitch (y) and roll (x) axis (maximum 1.9 degrees).

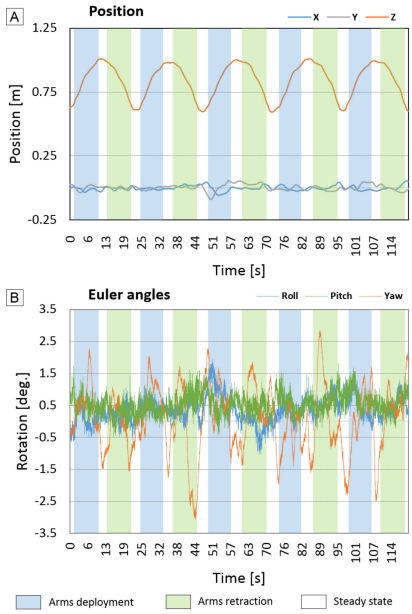

Fig. 12. Plots showing the stability of the drone's attitude and altitude during arms morphing. Colored areas show the different phases of morphing: the blue area – arm deployment; the green area – arm retraction; the white area – steady state between morphing. (A) Plot shows the drone's position in x, y, and z coordinates. (B) Plot shows the drone's attitude.

During morphing, the drone slowly rotates around its yaw axis to a maximum value of 3.25 degrees and subsequently returns to its original position. These experiments showed that the drone remains stable both in its position and in orientation during morphing. The test was repeated five times, producing similar results. These results, including the 0.3 m variation in altitude and small yaw oscillations, could be further improved by tuning the gains of the PID controller (rather than using the default values) to ensure that thrust can be adjusted quickly to maintain the altitude and orientation of the quadcopter.

E. Hovering Time

To show the difference in flight endurance between the retracted and deployed arm configurations, a test was conducted where the vehicle with a fully charged battery was commanded to keep a constant position and altitude of 1 m above the ground until the battery level reached 15% of full charge. The hovering time was measured five times in two different conditions: (i) fully retracted arms in the cage (average: 5 minutes 34 seconds, standard deviation: 4 seconds); (ii) deployed arms outside the cage (average: 8 minutes 3 seconds, standard deviation: 7 seconds). The experiment revealed that the drone with arms deployed

outside the cage can hover 31% longer before the battery reaches a 15% charge level.

V. Conclusion

We have described a novel approach to increase the safety and aerodynamic efficiency of an aerial delivery multicopter by using a compact, dense cage and morphing arms. The cage is made of a dense grid, which prevents fingers from accessing rotating propellers. During the short period of take-off and landing, the propellers are retracted into the cage to provide safety for people and the drone. During cruise flight at high altitude, the quadcopters arms deploy from the cage to increase aerodynamic efficiency. Arms deployed outside the cage increase lift by 0.606 kg, which is a 21% enhancement when compared with inside the cage (eliminating 10% and 11% of drag penalty of the cage and overlapping propellers, respectively). The mass of the components used to enable the arm deployment is 0.169 kg, which is 6% of the gross mass of the drone. This leads to a net lift saving of 15% or 0.437 kg compared to when the arms are retracted. This additional lift can be used to carry larger batteries or heavier payload. Moreover, placing the propellers and motors further apart from each other increases the stability of the quadcopter and decreases the control effort to maneuver the drone, which in turn leads to further energy savings. The weight of the cage is 0.377 kg, which is only 15% of the gross mass of the drone. From a design perspective, this weight penalty is reasonable (equivalent to the weight of battery component) considering the added safety for people and increased functionality provided with in-hand landing. Moreover, the cage could be optimized and the percentage value could be further reduced. The storage volume of the drone is reduced by 55% when the arms are retracted into the cage, which facilitates storage and transportation of the drone to the place of deployment.

Further weight reduction is possible by replacing the small plastic grids with larger modules. In addition, the frame holding the strings could be further strengthened by using carbon, aluminum alloy or titanium, similarly to the frame of tennis rackets.

Acknowledgment

The authors would like to thank Cameron Dowd for developing the propeller test bench, and Olexandr Gudozhnik for his assistance in the experiments with the motion capture system.

References

[1] D. Floreano and R. J. Wood, "Science, technology and the future of small autonomous drones," *Nature*, vol. 521, no. 7553, pp. 460–466, 2015.

[2] J. K. Stolaroff, C. Samaras, E. R. O'Neill, A. Lubers, A. S. Mitchell, and D. Ceperley, "Energy use and life cycle greenhouse gas emissions of drones for commercial package delivery," *Nature Commun.*, vol. 9, 2018, Art. no. 409.

[3] R. D'Andrea, "Guest editorial can drones deliver?" *IEEE Trans. Autom. Sci. Eng.*, vol. 11, no. 3, pp. 647–648, Jul. 2014.

[4] The Verge. "Alphabet's project wing drones will deliver burritos to australian homes," Jan. 2019. [Online]. Available: https://www.theverge.com/2017/10/16/16486208/alphbet-google-project-wing-drone-delivery-testing-australia

[5] Air, Amazon Prime. "Revising the airspace model for the safe integration of small unmanned aircraft systems," Jul. 2015. [Online]. Available: www.utm.arc.nasa.gov/docs/Amazon_Revising%20the%20Airspace%20Model%20for%20the%20Safe%20Integration%20of%20sUAS%5B6%5D.pdf

[6] "Swiss Post drone to fly laboratory samples for Ticino hospitals," Dec. 2017, [Online]. Available: https://www.post.ch/en/about-us/company/media/press-releases/2017/swiss-post-drone-to-fly-laboratory-samples-for-ticino-hospitals

[7] D. Moormann and Dieter. "DHL parcelcopter research flight campaign 2014 for emergency delivery of medication," in *Proc. ICAO RPAS Symp.*, 2015, p. 557. [Online]. Available: www.icao.int/Meetings/RPAS/RPASSymposiumPresentation/Day2Workshop5TechnologyDieterMoormann.pdf

[8] A. Klaptocz, A. Briod, L. Daler, J. C. Zufferey, and D. Floreano, "Euler spring collision protection for flying robots," in *Proc. IEEE Int. Conf. Intell. Robots Syst.*, 2013, pp. 1886–1892.

[9] A. Briod, P. Kornatowski, J. C. Zufferey, and D. Floreano, "A collision-resilient flying Robot," *J. F. Robot.*, vol. 31, no. 4, pp. 496–509, 2014.

[10] P. M. Kornatowski, S. Mintchev, and D. Floreano, "An origami-inspired cargo drone," in *Proc. IEEE Int. Conf. Intell. Robots Syst*, 2017, pp. 6855–6862.

[11] A. Kalantari and M. Spenko, "Design and experimental validation of HyTAQ, a hybrid terrestrial and aerial quadrotor," in *Proc. IEEE Internat. Conf. Robot. Autom.*, 2013, pp. 4445–4450.

[12] C. J. Salaan, K. Tadakuma, Y. Okada, E. Takane, K. Ohno, and S. Tadokoro, "UAV with two passive rotating hemispherical shells for physical interaction and power tethering in a complex environment," in *Proc. IEEE Int. Conf. Robot. Autom.*, 2017, pp. 3305–3312.

[13] C. J. Salaan, K. Tadakuma, Y. Okada, Y. Sakai, K. Ohno, and S. Tadokoro, "Development and experimental validation of aerial vehicle with passive rotating shell on each rotor," *IEEE Robot. Autom. Lett.*, vol. 4, no. 3, pp. 2568–2575, Jul. 2019.

[14] P. Abtahi, D. Y. Zhao, L. E. Jane, and J. A. Landay, "Drone near me: exploring touch-based human-drone interaction," in *Proc. ACM Interact. Mob. Wearable Ubiquitous Technol.*, vol. 1, no. 3, 2017, pp. 1–8.

[15] J. Salaan, Y. Okada, K. Hozumi, K. Ohno, and S. Tadokoro, "Improvement of UAV's flight performance by reducing the drag force of spherical shell," in *Proc. IEEE Int. Conf. Intell. Robots Syst.*, 2016, pp. 1708–171.

[16] R. Mahony, V. Kumar, and P. Corke, "Multirotor aerial vehicles: Modeling, estimation, and control of quadrotor," *IEEE Robot. Autom. Mag.*, vol. 19, no. 3, pp. 20–32, Sep. 2012.

[17] H. Maeda, M. Okauchi, and Y. Shimada, "A model for analysis of the impact between a tennis racket and a ball," *ISBS-Conf. Proc. Archive*, vol. 1, no. 1, pp. 35–38, Nov. 2000.

[18] ZooMed. "North American Box Turtle," Jul. 2019, [Online]. Available: https://zoomed.com/north-american-box-turtle/

[19] Project Noah. "Ornate Box Turtle," Jul. 2019, [Online]. Available: https://www.projectnoah.org/spottings/12040375

[20] D. M. Bramble, "Emydid shell kinesis: Biomechanics and evolution," in *Proc. Copeia*, 1974, pp. 707–727.

[21] P. M. Kornatowski, M. Feroskhan, W. Stewart, and D. Floreano, "Downside up: Rethinking parcel position for aerial delivery," *IEEE Robot. Autom. Lett.*, May 2020, doi: 10.1109/LRA.2020.2993768.

[22] B. Hohendorff *et al.*, "Lengths, girths, and diameters of children's fingers from 3 to 10 years of age," *Annals Anatomy-Anatomischer Anzeiger*, vol. 192, no. 3, pp. 156–161, 2010.

[23] S. Pheasent and C. M. Haslegrave, *Bodyspace: Anthropometry, Ergonomics and the Design of Work*, Boca Raton, FL, USA: CRC Press, 2018.

[24] R. G. Snyder, "Physical characteristics of children as related to death and injury for consumer product safety design," Rep. no. PB-242 221/0GA, May 1975, 241 pp; abstr in Government Reports Announcements ()." Applied Ergonomics 7.2: 112, 1976.

[25] L. Vilhena and A. Ramalho, "Friction of human skin against different fabrics for medical use," *Lubricants*, vol. 4, no. 1, 2016.

[26] G.J. Leishman, *Principles of Helicopter Aerodynamics With CD Extra*. Cambridge, U.K.: Cambridge Univ. Press, 2006.

[27] W. F. Lindsey, "Drag of cylinders of simple shapes," NACA. Boston, MA, USA, Annual Report 619, 1938.

[28] M. Mallick, A. Kumar, N. Tamboli, and A. Kulkarni, "Study on drag coefficient for the flow past a cylinder," *Int. J. Civil Eng. Res.*, vol. 5, no. 4, pp. 301–306, 2014.

[29] RCbenchmark.com. Mar. 2019, [Online]. Available: https://www.rcbenchmark.com/pages/series-1580-thrust-stand-dynamometer

[30] C. Y. Gooderson, D. J. Knowles, and P. M. Gooderson, "The hand anthropometry of male and female military personnel," APRE Memorandum 82M510, Army Personnel Research Establishment, Farnborough, Hants, 1982.

[31] E. Romero, R. Callupe and D. Elias, "Implementation of a finger force detection platform with a graphical user interface," in *Proc. IEEE 24th Int. Conf. Electron., Elect. Eng. Computing (INTERCON)*, 2017, pp. 1–4.